Tellurium Nanowires for Lithium-metal Anode Stabilization in High-performance Anode-free Li-S Batteries

*Hyunki Sul, Jiarui He, and Arumugam Manthiram**

Hyunki Sul, Dr. Jiarui He, Prof. Arumugam Manthiram*
Walker Department of Mechanical Engineering, The University of Texas at Austin, Austin, TX 78712, USA

Keywords: Lithium-sulfur batteries, tellurium nanowires, lithium-metal stabilization, separator coating, anode-free cell

ABSTRACT

Enhancing the reversibility of Li is crucial for extending the cycle life of Li-limited anode-free lithium-sulfur (Li-S) batteries. Incorporating tellurium (Te) in the system has proven to be highly effective by its reaction with polysulfides and forming a passivating interfacial layer on Li surface, which reduces Li-ion diffusion barrier. However, due to the poor utilization of Te, a significant amount of Te is required to improve cell cycling performance. To address this, tellurium nanowires (TeNW) are synthesized *via* a hydrothermal method and applied to Li_2S-based anode-free cells to minimize Te content in a system while extending the cell cycle life. Coating TeNW onto the separator greatly enhances Te utilization and demonstrates a significant cycle life improvement (38% retention over 300 cycles) with only 4 wt. % TeNW content relative to the active material. The versatility of TeNW is further demonstrated by utilizing it with carbon nanotubes as the anode substrate. The exceptional performance of TeNW is attributed to its high-surface area nanostructure and excellent conductive network, facilitating efficient electron transfer during cell cycling. These advantageous properties position TeNW as a promising material to enhance the cycle life of Li-limited Li-S batteries.

The exploration of new battery chemistries beyond lithium-ion batteries (LIBs) is imperative and essential to meet the growing market demands.[1–5] The limitations of current LIBs stem from the relatively low specific capacity (< 220 mA h g^{-1}) and the heavy weight of conventional transition-metal oxide cathodes. These factors restrict the specific energy density of LIBs within 250 W h kg^{-1}.[6–8] Meanwhile, lithium-sulfur (Li-S) batteries offer a high theoretical specific capacity of 1,675 mA h g^{-1} and can achieve a full-cell-level theoretical energy density of > 600 W h kg^{-1}.[9,10] Along with its high energy density, environmental friendliness, and cost-effectiveness, Li-S battery technology has garnered significant attention as a promising candidate for next-generation energy storage systems.[11–13]

In the Li-S system, the high theoretical capacity of sulfur necessitates the inclusion of a corresponding quantity of Li. Additionally, to compensate for Li loss caused by its reaction with electrolyte and formation of solid-electrolyte interphase (SEI) during cycling, an excess amount of Li is typically used in the system.[14–16] This excess Li is incorporated into the cell in the form of a thick Li-metal foil (with a thickness exceeding 500 μm), resulting in a negative-to-positive capacity (N/P) ratio greater than 20. However, such a high N/P ratio leads to an increase in excess Li weight, penalizing the specific energy of the Li-S battery to limit it to around 150 W h kg^{-1}.[17] Moreover, considering the rising price of Li, the inclusion of large quantities of Li in the cell undermines the cost-effectiveness advantage associated with Li-S batteries.[18,19] Consequently, there is a growing focus on approaches that aim to decrease the N/P ratio to achieve high energy density and low-price Li-S batteries.[20–23]

Among the various approaches to reduce the N/P ratio in Li-S batteries, anode-free full cells based on Li_2S cathodes have emerged as a promising avenue.[24–27] By combining a fully lithiated cathode with a bare current collector on the anode, it is possible to maintain the N/P ratio precisely

equal to 1.[28] Given the energy-, process-, and cost-intensive nature of manufacturing thin Li foils, the use of pre-lithiated Li_2S cathode-based anode-free cells presents notable advantages. First, they enable the maximum achievable energy density to be delivered without the presence of excess Li. Second, anode-free cells provide the flexibility to utilize various types of anodes, including carbon-based, silicon-based, and metal oxide-based materials to improve anode stability. Lastly, anode-free cells are free from self-discharging issues, as Li_2S cathodes start in a fully discharged state. These advantages make anode-free cells with pre-lithiated Li_2S cathodes a promising direction for research and development in advanced battery systems.

Nevertheless, the absence of excess Li in anode-free cells poses a challenge in terms of achieving extended cell cycle life. Numerous investigations have highlighted the prominent role of Li-metal anode degradation in determining the long-term cycling performance, particularly in Li-limited anode-free cell configurations.[29–32] Consequently, addressing the degradation issues associated with Li-metal anode is essential to optimize the performance and durability of anode-free cell systems. Several approaches have been attempted to improve the stability of the Li-metal anode, including the use of 3D hosts to enhance Li nucleation,[33–36] pre-treatments of the Li surface to minimize side reactions,[37–40] and *in-situ* solid-electrolyte interphase (SEI) modifications.[41–44] These strategies aim to mitigate the degradation mechanisms occurring at the Li-metal interface and improve the overall stability and cyclability of anode-free cells.

One effective approach to enhance the reversibility of the Li-metal anode is through the formation of a highly Li-ion conductive SEI layer. Instead of the conventional Li_2S-rich SEI, formation of ternary sulfide-rich SEI, such as Li_3PS_4, Li_2SnS_3, etc. has shown improved performance in terms of Li stripping & plating, as well as stability against polysulfides.[45–48] Especially, the inclusion of tellurium (Te) as the cathode additive has been found to significantly

enhance the cycling performance of anode-free cells by spontaneously reacting with polysulfides and forming a lithium polytellurosulfide ($Li_2Te_xS_y$)-rich SEI.[49] As Te being a group 16 element, it shares similar chemistry with sulfur, which makes it readily form $Li_2Te_xS_y$ compounds.[50] Additionally, Te has the ability to form soft Lewis acid cations (Te^{4+}), which have a preference for soft Lewis bases such as S^{2-} sulfides, favoring the formation of $Li_2Te_xS_y$ at the Li metal surface.[51,52] The presence of a superior Li-ion conductive SEI layer enables homogenous and dense Li morphology, which mitigates parasitic side reactions at the Li surface. Consequently, the Li inventory is well maintained throughout cell cycling.

However, in these studies, the use of commercial Te as a Li_2S cathode additive demonstrated cycle life improvement with an addition of approximately 20 wt. % Te. As widely known, Te is a heavy transition metal (127.6 g mol^{-1}) and an expensive material ($ 86.1 per kg).[53] Such an excess amount of Te addition in the Li-S system significantly diminishes the advantages of Li-S batteries in terms of gravimetric energy density and cost-effectiveness. Therefore, finding the optimal balance where Te content is minimized while effectively stabilizing the Li-metal anode is critical from a commercial viability standpoint. Ideally, by reducing Te content to less than 5 wt. % relative to Li_2S, the mass contribution of Te in the entire cell under practical pouch cells can be minimized to a mere 0.58 %, making it the lowest among all cell components (Table S1).

In this regard, what is the minimum Te content that can be reduced while still achieving significant cycling retention improvement in anode-free cells? To evaluate the impact of varying Te content at the cathode on cycling performance, commercial Te powder was mechanically mixed with Li_2S and carbon in different weight percentages; 10, 5, and 0 wt. %, and subsequently applied as a cathode material. Due to the ability of Te to stabilize the Li-metal anode, a Li-limited anode-free cell configuration was employed to effectively compare the impact of varying Te content in

the system. The Li_2S loading was 3 mg cm^{-2}, and 45 µL of electrolyte was injected. Since Li_2S was used as a cathode material, specific capacities are calculated on Li_2S basis.

As shown in Figure 1a, the conventional anode-free cell without Te shows a rapid capacity decay within 30 cycles, leading to a poor capacity retention of 11 % at the end of 100 cycles. When 5 wt. % of Te powder was added to the cathode, a slight cycle life improvement is detected (22 % retention over 100 cycles). To further enhance the cyclability of the cell, 10 wt. % of Te powder was applied to the cathode, resulting in a significant cycle life improvement (50 % retention over 100 cycles). Also, the increase in initial discharge capacity is detected, which might be coming from the catalytic effect of Te on sulfur redox.[54–57] Thus, it is apparent that achieving a meaningful improvement in anode-free cell performance necessitates a minimum of 10 wt. % of Te in the Li_2S cathode.

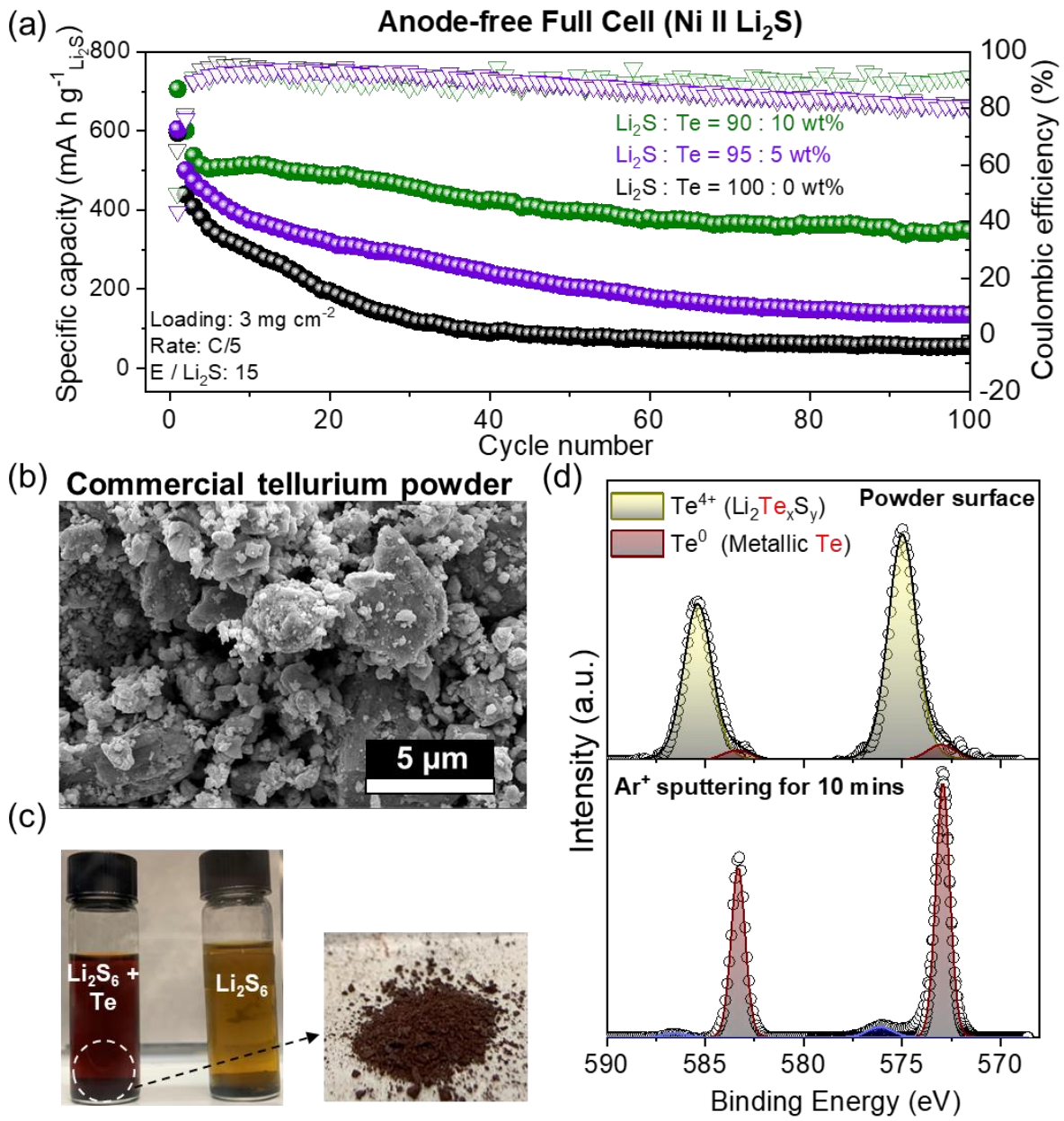

Figure 1. (a) Long-term cycling performance of anode-free Ni || Li_2S full cells with 10, 5, and 0 wt. % Te applied at the cathode compared to Li_2S. (b) SEM image of commercial Te powder. (c) Color change of Li_2S_6 when reacted with commercial Te powder and a digital image of dried Li_2S_6 + Te. (d) Te 3d XPS spectra of dried Li_2S_6 + Te at the surface and after 10 min of Ar^+ sputtering.

To investigate the origin of why a significant amount of Te is required, the reaction between commercial Te powder and lithium polysulfide was studied. As widely known, the mechanism of the Te stabilizing the Li-metal anode involves its reaction with lithium polysulfide, resulting in the

formation of a highly Li-ion conductive $Li_2Te_xS_y$ layer at the surface of Li-metal.[49,50] Scanning electron microscopy (SEM) image confirms that the commercial Te powder has a secondary particle size of up to ~ 5 μm (Figure 1b). When 0.01 M of the micron-sized Te powder got dispersed in 0.05 M Li_2S_6 solution in 1,3-dioxolane and 1,2-dimethoxyethane (DOL/DME), the change in color from yellow to red is detected. After drying out the supernatant, dark-red colored powder was collected, as shown in Figure 3c. This dark-red powder, which is known to be the color of polytellurosulfide ($Li_2Te_xS_y$) species, shows a spontaneous reaction between Te and Li_2S_6. X-ray photoelectron spectroscopy (XPS) analysis of the dried polytellurosulfide powder showed that Te is present as Te^{4+} at the surface of the powder (574.9 eV), which confirms the redox reaction between Te and Li_2S_6 (Figure 1d). The oxidation of Te from Te^0 to Te^{4+} is balanced by the reduction of S^0 to S^{1-} and S^{2-}, as shown in Figure S1. To analyze the bulk of the powder, Ar^+ sputtering of the surface was conducted for 10 min. Surprisingly, the resulting spectrum shows the disappearance of the reduced Te^{4+} peak and the emergence of metallic Te^0 peak at 572.9 eV. It is clearly shown that the reaction between Te and Li_2S_6 to form the $Li_2Te_xS_y$ only happened at the surface, and the bulk still remains as metallic Te^0.

A similar phenomenon is expected to occur inside the Li-S batteries. Upon cell cycling, micron-sized Te powder might mainly react with lithium polysulfides only at the surface, resulting in poor utilization of Te. The insulating nature of sulfur or Li_2S could exacerbate the low utilization of Te. In the end, an excess amount of Te is required to achieve cycling retention improvement. As mentioned earlier, the inclusion of a high content of Te within the system would offset the advantages of Li-S batteries, as Te is a heavy and costly metal. Therefore, to overcome the poor Te utilization, it is necessary to use the high-surface area structured Te to maximize its reaction with the polysulfides.

Typically, nanoscale materials exhibit a substantially higher surface area-to-volume ratio compared to their bulk counterparts, which results in shorter diffusion distances for electrons and Li-ions within the nanoparticles.[57–59] In particular, nanowires are well-known for their superior mechanical and thermal stability, as well as their excellent electrical conductivity.[60–62] It has been reported that the high-surface area nanowire structured material can be synthesized through the hydrothermal reaction.[63–65] Building upon this rationale, attempts have been made to synthesize Te materials in the form of nanowires, capitalizing on their unique structure.

Figure 1a illustrates the addition of Na_2TeO_3 as a Te source in deionized water, with polyvinylpyrrolidone (PVP) acting as a surfactant. After the solution was mixed for 30 minutes, hydrazine monohydrate and aqueous ammonia solution were introduced. The purpose of hydrazine is to mineralize and nano-crystalize the Te ions during the hydrothermal synthesis,[66,67] and ammonia contributes to preventing large Te crystal growth and improving the uniformity of the nanowire-structured Te.[68] Subsequently, the closed reaction vessel was subjected to a temperature ramp-up to 180 °C, creating high-temperature and high-pressure conditions to facilitate the hydrothermal process, which yields a nanowire-structured Te (TeNW). The elongated and rod-like nanowire structure was visualized with transmission electron microscopy (TEM), as shown in Figure 2b. The high magnification TEM image shows that the diameter of the nanowire is ~ 9 nm (Figure 2c). A well-resolved lattice fringes corresponds to the crystalline planes of hexagonal Te, whereas the amorphous region indicates the thin carbon coating at the surface. The source of carbon is coming from the reaction leftover from the PVP. The energy dispersive X-ray spectroscopy (EDX)-elemental mapping confirms the core of the nanowire is Te (green), whereas a surface coating consists of carbon (red), as shown in Figure 2d.

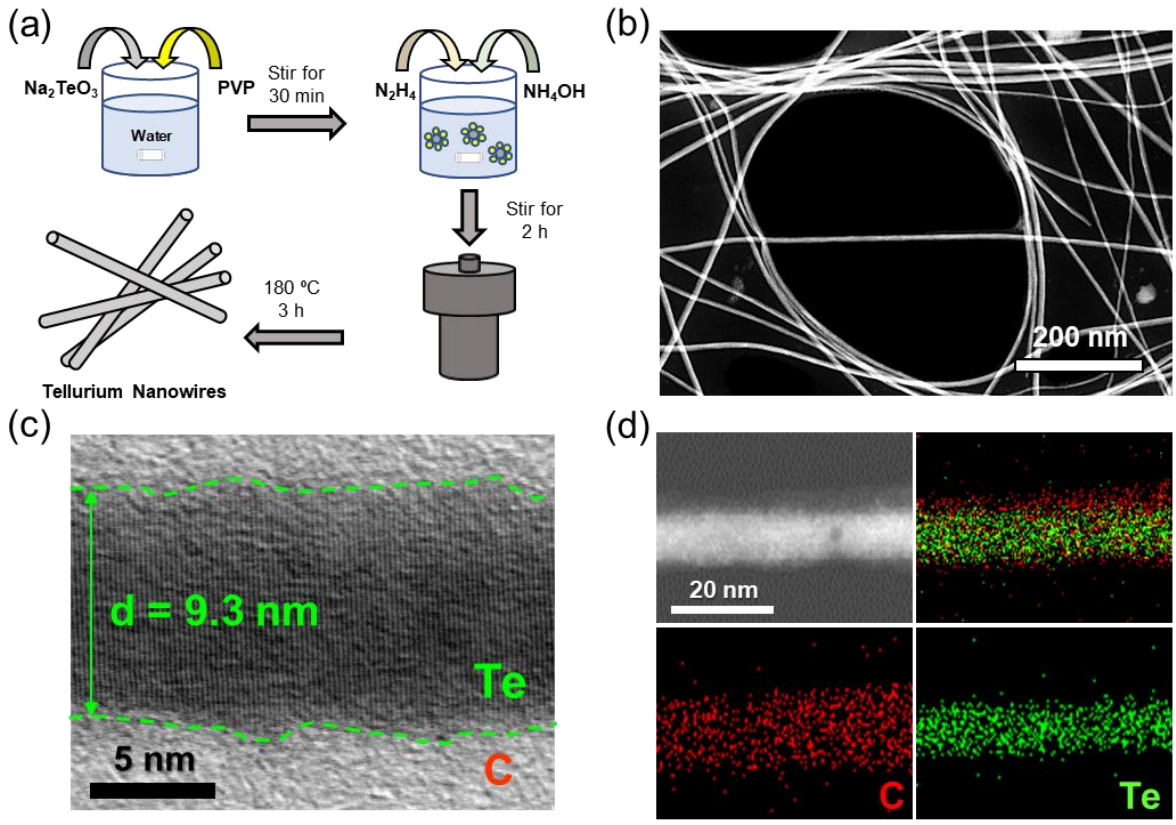

Figure 2. (a) Synthesis schematic of TeNW. (b) Low- and (c) high-magnification TEM image of TeNW. (d) EDX-elemental mapping of TeNW.

The amount of carbon coating on TeNW was quantified by thermogravimetric analysis (TGA) under N_2 atmosphere (Figure S2). In the temperature range of 450 ~ 520 ºC, weight loss is observed, which is attributed to the evaporation of Te. The content of carbon coating in the synthesized TeNW is found to be 10 wt. %. The crystalline structure of TeNW was further characterized with X-ray diffraction (XRD). As illustrated in Figure S3, TeNW exhibits distinct peaks corresponding to the hexagonal Te crystal structure, which aligns well with the standard data (JCPDS 36-1452). The series of material characterization reveals that the thin carbon-coated TeNW was successfully synthesized through the hydrothermal reaction.

To evaluate the potential application of TeNW in an anode-free Li-S system, 5 wt. % of TeNW was mechanically mixed with Li_2S and applied to the cathode. As shown in Figure S4, the

cell with TeNW exhibits an initial discharge capacity of 669 mA h g^{-1} with 29 % capacity retention at the end of 100 cycles, whereas the cell with the same wt. % of Te powder shows an initial capacity of 604 mA h g^{-1} with 22 % retention. Contrary to expectations, despite its high-surface area nanostructure, the cycling performance is not significantly improved with TeNW compared to the same wt. % of Te powder. It is assumed that even with an increased surface area of nanostructured Te, the insulating characteristics of Li_2S play a dominant role in impeding the utilization of TeNW. Note that the ultimate goal is to discover a strategy to enhance cell cycling performance in the Li-S system while minimizing the Te content. Therefore, adding TeNW into a cathode composed of Li_2S with poor ionic and electronic conductivity may not be an effective strategy.

An alternative approach to incorporate TeNW into the Li-S system is by coating it onto the separator. Separator coating offers the advantage of isolating TeNW from the insulating Li_2S and allows for an easy application of the existing slurry coating method from a manufacturing standpoint. It is expected that during cell cycling, polysulfides dissolved in the electrolyte can spontaneously react with TeNW at the separator and migrate to Li-metal anode to form a favorable SEI layer (Figure 3a). TeNW was homogenously mixed with commercial Soteras binder (95: 5 wt. %) in water and subsequently blade-casted onto Celgard 2500 separator. The TeNW has a nano-sized diameter and a rod-like structure, which enables a uniform and thin coating in a wide area of the separator. SEM image shows a homogenous distribution of the TeNW coating at the surface of the separator (Figure S5) and the thickness of the coating is ~ 7.3 μm (Figure S6).

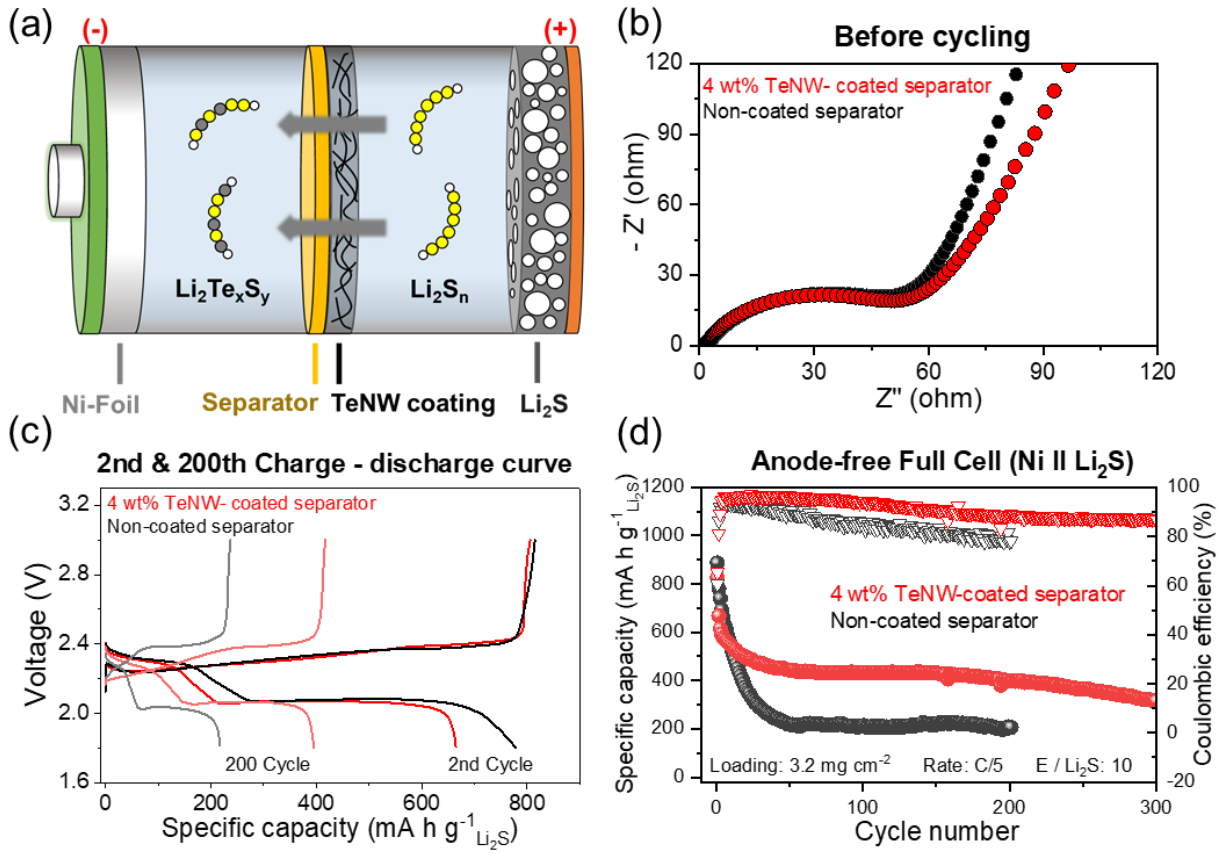

Figure 3. (a) Schematic of the TeNW-coated separator in anode-free cell configuration. (b) Nyquist plots before cycling, (c) 2nd and 200th cycle charge-discharge curves, and (d) long-term cycling performance of 4 wt. % TeNW-coated separator and uncoated separator cells.

The TeNW-coated separator was combined with Li_2S cathode in an anode-free cell configuration to evaluate the electrochemical performance. Li_2S loading was 3.2 mg cm^{-2} and the total mass of TeNW that were coated onto the separator was 0.13 mg cm^{-2}. The content of TeNW was purposely controlled to a low percentage of 4 wt. % compared to Li_2S in the cell. To measure the increase in cell resistance that may occur due to the separator coating, electrochemical impedance spectroscopy (EIS) was conducted. Despite the addition of a new layer consisting of TeNW to the separator, the charge-transfer resistance of the pristine cells does not show a significant difference compared to the uncoated case, as shown in Figure 3b. This result is also observed in the charge-discharge curves of the 2nd cycle. Based on Figure 3c, the cell with the TeNW coating shows a similar voltage polarization as the cell without Te coating. The results

from the EIS and voltage curve analysis suggest that the ultra-thin TeNW layer at the separator does not significantly increase the cell resistance or hinder the reaction kinetics.

To compare the cell performance based on the separator coating side, two configurations were examined: one with the coating side facing the cathode and the other with the coating side facing the anode, as depicted in Figure S7a. From the cycling performance shown in Figure S7b, the TeNW-coated side facing the cathode shows slightly better capacity retention and higher average coulombic efficiency (67 % retention, 93.0 % coulombic efficiency) compared to the cell with the TeNW-coated side facing the anode (63 % retention, 91.9 % coulombic efficiency) throughout 30 cycles. The exposure of TeNW-coated side towards the cathode might have maximized the reaction between TeNW and polysulfides to form polytellurosulfide species, which facilitates the generation of stable SEI on Li surface. Moving forward, all cells were assembled with the TeNW-coated side facing the cathode, considering the superior cycling performance observed in this configuration.

The enhanced cycling stability attributed to the TeNW was confirmed through a long-term cycling performance measurement conducted at C/10 rate activation for 3 cycles, followed by C/5 rate. Figure 3d shows that regardless of a low TeNW content of 4 wt. % in the system, the anode-free cell delivers good cycle life improvement at the end of 300 cycles (316 mA h g^{-1}, 38 % retention), exhibiting a small capacity decay of 1.7 mA h g^{-1} per cycle with an average coulombic efficiency of 91.3 %. The initial capacity fade during the first 5 cycles is attributed to the consumption of S and Li during the formation of a robust SEI, after which the cell exhibits excellent capacity retention. The gradual attenuation of Te signal on the coated separator, as shown in Figure S8, reveals the consumption of Te by reaction with the polysulfides to form a stable SEI. In contrast, the control cell without the Te in the system shows a rapid capacity decay, losing

almost 75 % of its capacity within the first 50 cycles and exhibiting a lower average coulombic efficiency of 85.3 %. Thus, it is shown that the application of TeNW on the separator is an effective way to significantly improve cell cycling performance, while reducing Te content down to 4 wt. %.

One important aspect to consider is whether the improvement in cell cycling performance is attributed to TeNW itself or by the additional separator coating. As widely known, the addition of a layer on the separator might have some degree of suppression of shuttle effect by physically anchoring the polysulfides, which can improve the cycling performance of anode-free cells. Even though the TeNW on the separator seems to disappear during cycling, the binder used to coat the separator may remain in the separator and potentially have an impact on suppressing polysulfide shuttling. To investigate whether the binder itself has any polysulfide shuttle-suppressing effect, a shuttle current test was conducted where only the binder was coated onto the separator without the addition of TeNW. As shown in Figure S9, both the coated separator and the uncoated separator cell show a similar shuttle current of ~ 0.11 mA, which indicates that the binder itself used on the separator coating has negligible impact on the suppression of polysulfide migration. It is confirmed that the dominant mechanism for improving the cell cycling retention is not by the separator coating itself, but by the TeNW.

For a direct comparison with TeNW, commercial Te powder was also coated on the separator using the same binder. The uneven particle size distribution of Te powder hampers the homogenous mixing with the binder. Thus, carbon was needed to enable the Te powder coating onto the separator. As shown in Figure S10a, the separator coated with Te powder exhibits irregular Te and carbon distribution. Additionally, the commercial Te powder has a large particle size, which limits the minimum achievable coating thickness to approximately 12 μm (Figure S10b). Due to the substantial coating thickness, when combined with a 3.2 mg cm^{-2} loading of a

Li_2S cathode, the total Te content turned out to be 15 wt. % relative to Li_2S. It is well known that such irregularity in the separator coating can lead to an inhomogeneous Li-ion flux, resulting in non-uniform Li stripping and plating at the anode. Furthermore, thicker separator coating causes an ohmic drop in the cell, which causes increased voltage polarization and larger charge-transfer resistance, as shown in Figure S11a and Figure S11b. Although the Te powder-coated separator cells contained a high Te content of 15 wt. %, the cells did not exhibit a dramatic improvement in cycling stability compared to the control cell (Figure S12). Based on these results, it can be concluded that using TeNW instead of Te powder is a better choice to apply it to the separator and achieve the most efficient cycling performance enhancement while minimizing the Te content.

In order to understand the effects of the TeNW-coated separator on the anode side, the deposited Li in anode-free full cells after 30 cycles were analyzed. SEM image shows that Li cycled with TeNW-coated separator reveals a dense, planar, and smooth morphology (Figure 4a). The red-colored areas generated on Li-metal surface (Figure 4a inset image) indicate the formation of a SEI layer containing lithium polytellurosulfides. In contrast, Li with conventional uncoated separator shows mossy and filamentous deposition (Figure 4b). The contrasting Li morphologies help explain the differences in capacity retention observed in Figure 3d. The mossy deposition of Li leads to severe parasitic side reaction between Li with electrolyte to form a “dead” metallic Li. In contrast, the dense and uniform morphology of Li minimizes the reaction sites to preclude such an irreversible loss of Li inventory during cycling.

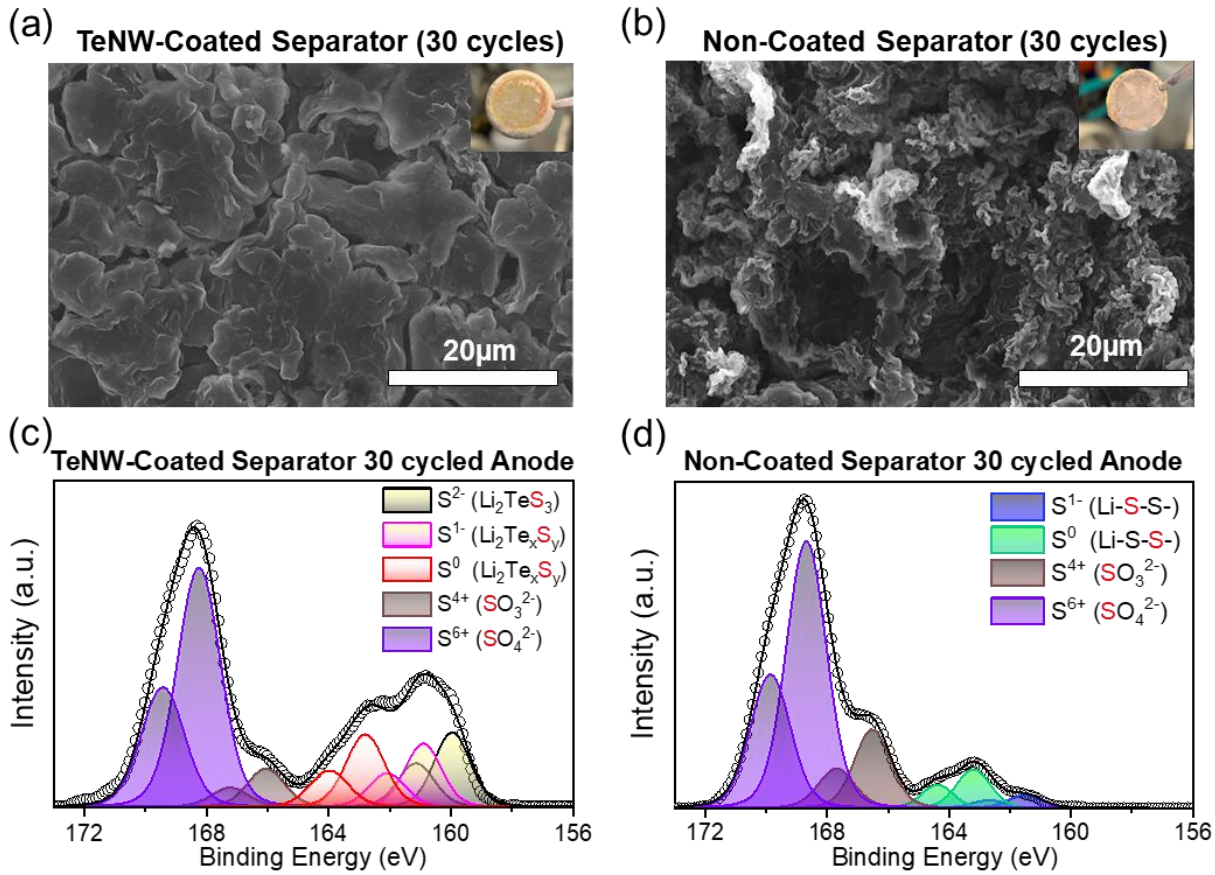

Figure 4. SEM images of Li-metal anode surfaces after 30 cycles: (a) TeNW-coated separator cell and (b) uncoated separator cell. The insets are the digital images of Li-plated Ni-foils from the anode-free cells after 30 cycles. S 2p XPS spectra of Li-metal surface after 30 cycles: (c) TeNW-coated separator cell and (d) uncoated separator cell.

To determine the underlying cause of the contrasting Li morphologies, the chemical composition of the SEI layer after 30 cycles was analyzed with XPS. Figure 4c presents the S 2p spectra of the Li surface for the cell with the TeNW-coated separator. It is shown that reduced sulfide peaks (S^{2-}) are detected at 159.9 eV, indicating the formation of Li_2TeS_3 at the surface of Li-metal anode.[49] Additionally, the peaks of terminal sulfur (S^{1-}) and bridging sulfur (S^0) at 160.9 eV and 162.8 eV, respectively, suggests the presence of intermediate polytellurosulfide species. It has been reported that the Te containing ternary sulfide ($Li_2Te_xS_y$) species at the SEI acts as a good Li-ion conductor to efficiently distribute the Li-ion flux, leading to a homogenous Li plating and stripping.[51,69]

The formation of reaction products between Te and polysulfides can also be confirmed from the Te 3d XPS spectra. Figure S13 shows the presence of Te^{4+} peaks at 574.8 eV on the surface of the SEI, which results from the formation of Li_2TeS_3. Tellurium oxide peaks at 575.5 eV might be coming from the reaction between Te and the electrolyte. To confirm the nature of the SEI layer containing Te, Ar^+ sputtering was conducted for 10 min. As it gets closer to the bulk deposited Li, the strongly reducing nature of Li metal leads to a further reduction in Te into Te^{1-} (Li_2Te_2) or Te^{2-} (Li_2Te), which are shown in the peaks at 571.7 eV and 569.9 eV, respectively. The transition from Li_2TeS_3 to Li_2Te_2 and Li_2Te, as getting closer to bulk Li metal, shows a similar trend as in the literatures.[49,50] XPS spectra clearly reveal that the TeNW from the separator undergoes the reaction with polysulfides and migrates to the Li-metal anode to form a good Li-ion conducting SEI layer.

In contrast, the cycled cell with a conventional uncoated separator shows a distinctive S 2p spectrum. As shown in Figure 4d, the peaks of terminal sulfur S^{1-} at 161.4 eV and bridging sulfur S^0 at 163.16 eV are known to be coming from the lithium polysulfides. The dominating intensity of oxidized sulfur species (S^{4+}, S^{6+}) indicates that severe electrolyte decomposition is taking place at Li surface. Such a difference in SEI chemical composition and resulting Li-metal morphological changes observed in this study are consistent with previous reports. Compared to the conventional binary sulfide (Li_2S)-rich SEI, the ternary sulfide ($Li_2Te_xS_y$)-rich SEI has a highly covalent characteristic due to the small electronegativity difference between S (2.58) and Te (2.10). As a result, the ternary sulfide ($Li_2Te_xS_y$)-dominant SEI leads to a low Li-ion diffusion barrier, allowing for smoother Li-ion transport. Consequently, Li-ion flux becomes more uniform, which facilitates a homogenous Li plating and stripping processes, as demonstrated in Figure 5. Therefore, coating

the separator with TeNW can provide analogous stabilizing effect on the Li-metal anode as the previously reported mechanisms with a much lower TeNW content of only 4 wt. % in the system.

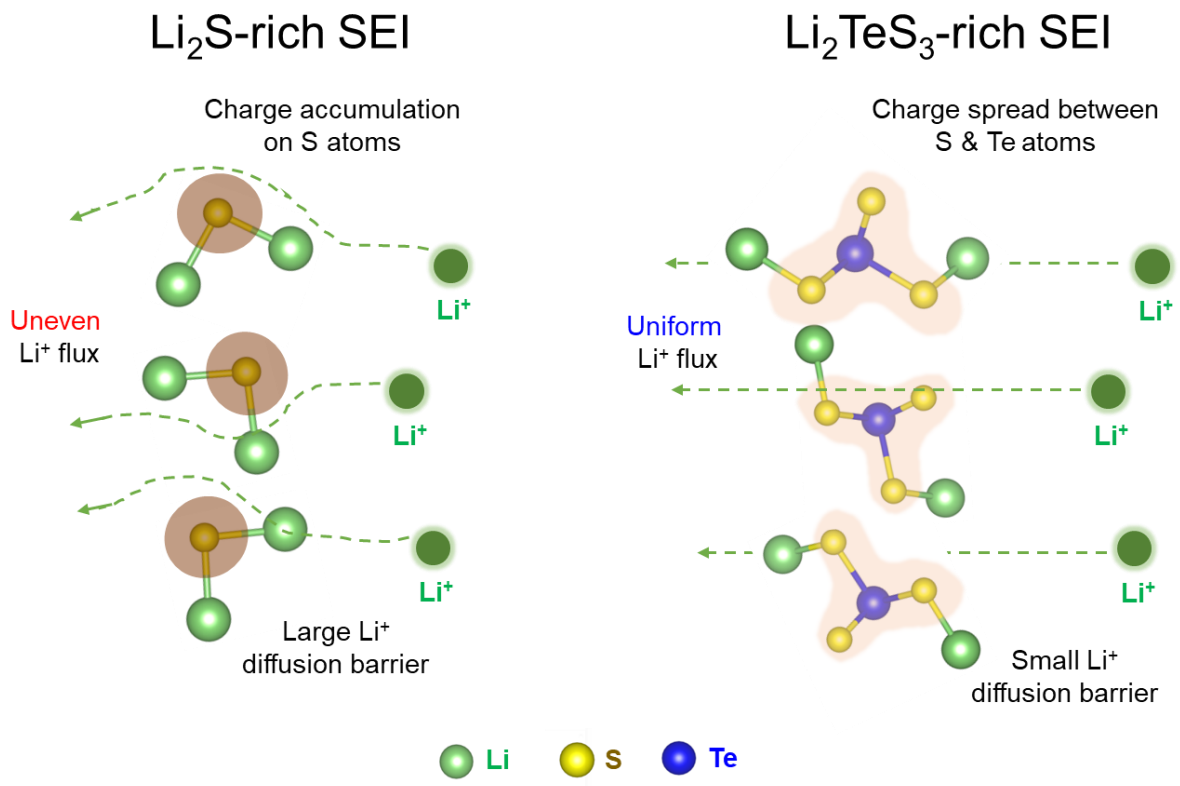

Figure 5. Schematic of the Li-ion diffusion trend in conventional Li_2S-rich SEI and Li_2TeS_3-rich SEI.

To further demonstrate the universal applicability of TeNW in Li-S system, the possibility of applying TeNW to other cell components was investigated. Since the mechanism by which TeNW enhances cell cycle life mainly occurs at the Li-metal anode, direct application of TeNW to the anode can be an effective approach. Based on this motivation, a method of using TeNW with carbon nanotube (CNT) as an anode substrate was attempted. The TeNW and CNT in a 1 : 9 weight ratio were dispersed in ethanol / water (1:1 vol %) solution *via* probe-sonication and subsequently vacuum filtered to form a binder-free TeNW @ CNT sheet (Figure S14). The XRD pattern of the TeNW @ CNT sheet reveals a dominating carbon peak around 26°, and small peaks

at 38.5°, 40.5°, and 49.7° which correspond to a crystalline Te (Figure S15). To utilize the TeNW @ CNT sheet as a Li-metal anode substrate, a pre-lithiation process was carried out. A controlled amount of Li was electrodeposited onto TeNW @ CNT to uniformly distribute Li on the free-standing sheet (Figure S16a). The amount of Li deposited on the Li-TeNW @ CNT was intentionally controlled to match the N/P ratio of 1, which is the same N/P ratio as the previously used Li_2S cathode-based anode-free cells. Subsequently, the pre-lithiated Li-TeNW @ CNT was assembled with a sulfur cathode at a loading of 3.2 mg cm^{-2}, as shown in Figure S16b. The total amount of TeNW applied to the Li-TeNW @ CNT was 0.2 mg cm^{-2}, which corresponds to 4 wt. % compared to the weight of Li and S in the cell when converted to the mass of Li_2S.

Pre-lithiated Li-TeNW @ CNT combined with the sulfur cathode was cycled to evaluate the long-term cycling performance. For the control cell, CNT without TeNW was vacuum filtered to make the free-standing sheet and pre-lithiated to act as an anode (Li-CNT). Since the cathode started with the elemental sulfur, the specific capacities are calculated on the basis of the mass of sulfur. Figure S17 demonstrates that the cell containing TeNW in the anode substrate exhibit a significant capacity retention of 57 % (532 mA h g^{-1}) after 200 cycles with a stable average coulombic efficiency of 91.7 %. In contrast, the control cell without TeNW in the system exhibits a rapid capacity decay after 50 cycles and shows a capacity retention of only 5 % (42 mA h g^{-1}) after 200 cycles with a poor average coulombic efficiency of 85.4 %. It is worth emphasizing that good cycling performance of these cells is achieved when Li and S are stoichiometrically balanced without excess lithium (N/P = 1). Therefore, it is shown that directly applying TeNW to the anode side can also effectively improve cycling performance with low Te content, as demonstrated in this study. The universal applicability of TeNW, not only as a coating material for separators but

also as an anode substrate, can be a promising strategy to increase the lifespan of Li-limited low N/P ratio Li-S batteries.

In summary, various strategies incorporating TeNW into the system have been proven to significantly increase the lifespan of Li-limited Li-S batteries. The nano-sized high surface area property of TeNW has shown that it can effectively enhance the cell cycle life even with a low Te content. In addition, by isolating TeNW from electronically and ionically insulating sulfur or Li_2S cathodes and incorporating them into the separator or anode side, the utilization of Te can be maximized, leading to an enhanced cyclability with a low TeNW content of only 4 wt. % relative to the active material. TeNW plays a similar role in stabilizing the Li-metal side as the existing Te mechanism by forming a good Li-ion conductive SEI containing polytellurosulfides ($Li_2Te_xS_y$) on Li surface. Therefore, it contributes to a dense and uniform deposition of Li metal, ultimately resulting in an innovative increase in cycle life, especially in Li-limited systems. This work provides a rational design strategy to realize high-energy density long cycle life anode-free Li-S batteries.

ASSOCIATED CONTENT

Supporting Information

The Supporting Information is available for this paper at

Competing interests

The authors declare no competing interest.

ACKNOWLEDGMENTS

This work was supported by the National Science Foundation, Division of Chemical, Bioengineering, Environmental, and Transport Systems, under award number 2011415

REFERENCES

[1] J. W. Choi, D. Aurbach, *Nat. Rev. Mater.* **2016**, *1*, 16013.

[2] S. Chu, Y. Cui, N. Liu, *Nat. Mater.* **2017**, *16*, 16.

[3] B. Dunn, H. Kamath, J. M. Tarascon, *Science.* **2011**, *334*, 928.

[4] Y. Fei, Y. Man, J. Sun, Y. Du, B. Chen, J. Bao, X. Zhou, *Small.* **2023**, 2301954.

[5] Y. Xu, T. Ding, D. Sun, X. Ji, X. Zhou, Y. Xu, T. Ding, D. Sun, X. Zhou, X. Ji, *Adv. Funct. Mater*. **2023**, *33*, 2211290.

[6] D. Lin, Y. Liu, Y. Cui, *Nat. Nanotechnol.* **2017**, *12*, 194.

[7] Y. Guo, H. Li, T. Zhai, *Adv. Mater.* **2017**, *29*, 1700007.

[8] A. Manthiram, *Nat. Commun.* **2020**, *11*, 1550.

[9] A. Manthiram, Y. Fu, S. H. Chung, C. Zu, Y. S. Su, *Chem. Rev.* **2014**, *114*, 11751.

[10] G. Zhou, H. Chen, Y. Cui, *Nat. Energy* **2022**, *7*, 312.

[11] Y. Chen, T. Wang, H. Tian, D. Su, Q. Zhang, G. Wang, *Adv. Mater.* **2021**, *33*, 2003666.

[12] S.-H. Chung, A. Manthiram, *Adv. Mater.* **2019**, *31*, 1901125.

[13] Z. Qu, X. Zhang, R. Xiao, Z. Sun, F. Li, Acta Phys. -Chim. Sin. **2023**, *39(8)*, 2301019.

[14] S.-H. Chung, A. Manthiram, *Adv. Mater.* **2018**, *30*, 1705951.

[15] X. Yu, A. Manthiram, *Acc. Chem. Res.* **2017**, *50*, 2653.

[16] W. Xu, J. Wang, F. Ding, X. Chen, E. Nasybulin, Y. Zhang, J. G. Zhang, *Energy Environ. Sci.* **2014**, *7*, 513.

[17] A. Bhargav, J. He, A. Gupta, A. Manthiram, *Joule* **2020**, *4*, 285.

[18] J. Sun, T. Wang, Y. Gao, Z. Pan, R. Hu, J. Wang, *InfoMat* **2022**, *4*, e12359.

[19] N. Bourlioufas, Lithium prices to keep rising as demand outpaces supply. <https://www.afr.com/wealth/investing/lithium-prices-to-keep-rising-as-demand-outpaces-supply-20230508-p5d6m3>, (Accessed 15 May 2023)

[20] X. B. Cheng, C. Yan, J. Q. Huang, P. Li, L. Zhu, L. Zhao, Y. Zhang, W. Zhu, S. T. Yang, Q. Zhang, *Energy Storage Mater.* **2017**, *6*, 18.

[21] W. Lu, Z. Wang, G. Sun, S. Zhang, L. Cong, L. Lin, S. Chen, J. Liu, H. Xie, Y. Liu, *J. Energy Chem.* **2023**, *80*, 32.

[22] M. Zhao, B. Q. Li, H. J. Peng, H. Yuan, J. Y. Wei, J. Q. Huang, *Angew. Chemie Int. Ed.* **2020**, *59*, 12636.

[23] O. Leonet, Á. Doñoro, A. Fernández-Barquín, A. Kvasha, I. Urdampilleta, J. A. Blázquez, *Front. Chem.* **2022**, *10*, 420.

[24] J. Chen, J. Xiang, X. Chen, L. Yuan, Z. Li, Y. Huang, *Energy Storage Mater.* **2020**, *30*, 179.

[25] J. He, A. Bhargav, A. Manthiram, *ACS Energy Lett.* **2022**, *7*, 583.

[26] D. Su, D. Zhou, C. Wang, G. Wang, *Adv. Funct. Mater.* **2018**, *28*, 1800154.

[27] S. Nanda, A. Gupta, A. Manthiram, *Adv. Energy Mater.* **2018**, *8*, 1801556.

[28] S. Nanda, A. Gupta, A. Manthiram, *Adv. Energy Mater.* **2021**, *11*, 2000804.

[29] C. J. Huang, B. Thirumalraj, H. C. Tao, K. N. Shitaw, H. Sutiono, T. T. Hagos, T. T. Beyene, L. M. Kuo, C. C. Wang, S. H. Wu, W. N. Su, B. J. Hwang, *Nat. Commun.* **2021**, *12*, 1452.

[30] S. Nanda, A. Manthiram, *Energy Environ. Sci.* **2020**, *13*, 2501.

[31] A. J. Louli, A. Eldesoky, R. Weber, M. Genovese, M. Coon, J. deGooyer, Z. Deng, R. T. White, J. Lee, T. Rodgers, R. Petibon, S. Hy, S. J. H. Cheng, J. R. Dahn, *Nat. Energy.* **2020**, *5*, 693.

[32] L. Su, H. Charalambous, Z. Cui, A. Manthiram, *Energy Environ. Sci.* **2022**, *15*, 843.

[33] J. He, A. Bhargav, H. Sul, A. Manthiram, *Angew. Chemie Int. Ed.* **2023**, *62*, e202216267.

[34] C. Wei, Y. Wang, Y. Zhang, L. Tan, Y. Qian, Y. Tao, S. Xiong, J. Feng, *Nano Res.* **2021**, *14*, 3576.

[35] Z. Yang, Q. Ruan, Y. Xiong, X. Gu, *Batter.* **2022**, *9*, 30.

[36] S. Lin, M. K. Shafique, Z. Cai, J. Xiao, Y. Chen, Y. Wang, X. Hu, *ACS Nano.* **2019**, *13*, 13037.

[37] M. Wu, Z. Wen, J. Jin, B. V. R. Chowdari, *ACS Appl. Mater. Interfaces.* **2016**, *8*, 16386.

[38] J. Luo, C.-C. Fang, N.-L. Wu, *Adv. Energy Mater.* **2018**, *8*, 1701482.

[39] G. Zheng, C. Wang, A. Pei, J. Lopez, F. Shi, Z. Chen, A. D. Sendek, H. W. Lee, Z. Lu, H. Schneider, M. M. Safont-Sempere, S. Chu, Z. Bao, Y. Cui, *ACS Energy Lett.* **2016**, *1*, 1247.

[40] N. Delaporte, Y. Wang, K. Zaghib, *Front. Mater.* **2019**, *6*, 267.

[41] X. Liang, Z. Wen, Y. Liu, M. Wu, J. Jin, H. Zhang, X. Wu, *J. Power Sources.* **2011**, *196*, 9839.

[42] S. Liu, G. R. Li, X. P. Gao, *ACS Appl. Mater. Interfaces.* **2016**, *8*, 7783.

[43] F. Wu, J. T. Lee, N. Nitta, H. Kim, O. Borodin, G. Yushin, O. Borodin, *Adv. Mater.* **2015**, *27*, 101.

[44] M. Liu, Y. Ren, H. Jiang, C. Luo, F. Y. Kang, T. S. Zhao, *Nano Energy*. **2017**, *40*, 240

[45] Y. Ren, A. Bhargav, W. Shin, H. Sul, A. Manthiram, *Angew. Chemie Int. Ed.* **2022**, *61*, e202207907.

[46] K. Homma, M. Yonemura, T. Kobayashi, M. Nagao, M. Hirayama, R. Kanno, *Solid State Ionics.* **2011**, *1*, 53.

[47] Q. Pang, X. Liang, A. Shyamsunder, L. F. Nazar, *Joule.* **2017**, *1*, 871.

[48] H. Sul, A. Bhargav, A. Manthiram, *Adv. Energy Mater.* **2022**, *12*, 2200680.

[49] S. Nanda, A. Bhargav, A. Manthiram, *Joule.* **2020**, *4*, 1121.

[50] S. Nanda, A. Bhargav, Z. Jiang, X. Zhao, Y. Liu, A. Manthiram, *Energy Environ. Sci.* **2021**, *14*, 5423.

[51] G. Sahu, Z. Lin, J. Li, Z. Liu, N. Dudney, C. Liang, *Energy Environ. Sci.* **2014**, *7*, 1053.

[52] Y. Wang, X. Lü, C. Zheng, X. Liu, Z. Chen, W. Yang, J. Lin, F. Huang, *Angew. Chemie*

2019, *131*, 7755.

[53] Daily Metal Price: Tellurium Price (USD / Kilogram) Chart for the Last 5 Years. < https://www.dailymetalprice.com/metalpricecharts.php?c=te&u=kg&d=240>, (Accessed 15 May 2023)

[54] X. Song, D. Tian, Y. Qiu, X. Sun, B. Jiang, C. Zhao, Y. Zhang, L. Fan, N. Zhang, *Energy Storage Mater.* **2021**, *41*, 248.

[55] X. Wen, F. Zeng, F. Shao, H. Li, *J. Electron. Mater.* **2023**, *52*, 2292.

[56] K. Xu, X. Liu, J. Liang, J. Cai, K. Zhang, Y. Lu, X. Wu, M. Zhu, Y. Liu, Y. Zhu, G. Wang, Y. Qian, *ACS Energy Lett.* **2018**, *3*, 420.

[57] Z. Song, W. Jiang, X. Jian, F. Hu, *Nanomater.* **2022**, *12*, 4341.

[58] M. A. Weret, W. N. Su, B. J. Hwang, *Batter. Supercaps* **2022**, *5*, e202200059.

[59] J. Balach, J. Linnemann, T. Jaumann, L. Giebeler, *J. Mater. Chem. A* **2018**, *6*, 23127.

[60] T. Tang, T. Zhang, L. Zhao, B. Zhang, W. Li, J. Xu, T. Li, L. Zhang, H. Qiu, Y. Hou, *Sci China Mater* **2020**, *2020*, 1910.

[61] L. Huang, Q. Wei, R. Sun, L. Mai, *Front. Energy Res.* **2014**, *2*, 43.

[62] L. N. Quan, J. Kang, C. Z. Ning, P. D. Yang, J. Deng, Y. Su, D. Liu, B. Liu, C. Liu, *Chem. Rev.* **2019**, *119*, 8955.

[63] B. Liu, H. C. Zeng, *J. Am. Chem. Soc.* **2003**, *125*, 4430.

[64] B. Bari, J. Lee, T. Jang, P. Won, S. H. Ko, K. Alamgir, M. Arshad, L. J. Guo, *J. Mater. Chem. A.* **2016**, *4*, 11365.

[65] J. He, Y. Chen, W. Lv, K. Wen, Z. Wang, W. Zhang, Y. Li, W. Qin, W. He, *ACS Nano* **2016**, *10*, 8837.

[66] X. Yu, X. An, *Mater. Lett*. **2010**, *64*, 252.

[67] A. Mahieddine, L. Adnane-Amara, *J. Electroanal. Chem*. **2023**, *930*, 117168.

[68] Y. Zhang, M. Cui, H. Wang, Z. Zhao, L. Wang, Y. Hou, *J. Rare Earths*. **2021**, *39*, 419.

[69] G. Lu, C. Ye, W. Li, X. He, G. Chen, J. Li, H. Jin, S. Wang, J. Wang, *Front. Chem.* **2021**, *9*, 377.

TABLE OF CONTENTS / ABSTRACT GRAPHIC

High surface area nanostructured tellurium nanowires utilized in lithium-limited Li-S full cells enhance the cycling performance by stabilizing the Li-metal anode. Coating the nanowires on the separator or using them as an anode substrate maximizes tellurium utilization, resulting in improved cycle life with minimal tellurium content.

*Hyunki Sul, Jiarui He, and Arumugam Manthiram**

Tellurium Nanowires for Lithium-metal Anode Stabilization in High-performance Anode-free Li-S Batteries

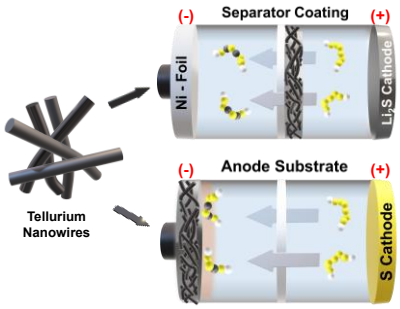

Supporting Information

Tellurium Nanowires for Lithium-metal Anode Stabilization in High-performance Anode-free Li-S Batteries

*Hyunki Sul, Jiarui He, and Arumugam Manthiram**

Experimental Section

Synthesis and preparation of Tellurium nanowire (TeNW)

0.178 g of Na_2TeO_3 and 2 g of polyvinylpyrrolidone (PVP) were dissolved in 50 mL of deionized water for 30 min. 3.3 mL of hydrazine monohydrate and 7.1 mL of aqueous ammonia solution were added and further stir-mixed for 2 h at room temperature. The solution was transferred into a polytetrafluoroethylene hydrothermal container and heated up to 180 ºC for 3 h at a ramp rate of 4 ºC min^{-1}. After cooling down the container to room temperature, the TeNW samples could be precipitated by adding an appropriate amount of acetone into the solution, washing with acetone several times, and drying in vacuum at 60 ºC.

Preparation of Li_2S cathodes

Commercial Li_2S (99.9 % metal basis, Sigma Aldrich), multi-walled carbon nanotubes (MWCNT, Nanostructured & Amorphous Materials Inc.), and Super-P were dry milled for 2 h with a long roll jar-milling system (US Stoneware 802 CVM) in a weight % ratio of 80: 10: 10. The resulting homogenously mixed composite was wet ball milled in a PTFE bottle with a mixture of 90 wt. % composite and 10 wt. % PEO/PVP binder in a 1,2-dimethoxyethane (DME), 1,4-dioxane, and acetonitrile solution media for 24 h. Yttria-stabilized zirconia (YSZ) grinding balls

were used to create a uniform slurry mixture. The slurry was blade casted onto an aluminum foil, and the electrode was dried inside an argon-filled glovebox under vacuum for 24 h to remove the solvent. Cathodes with a Li_2S loading of ~ 3 mg cm^{-2} and a Li_2S content of 72 wt. % were obtained. Commercial tellurium (Te, Sigma Aldrich) or TeNW was added to the slurry mixture in a weight ratio of 90: 10 and 95: 5 with Li_2S and blade casted onto an aluminum foil.

Preparation of Sulfur cathodes

Commercial S (99.5+%, Acros Organics) was melt-diffused into Ketjen Black (KB, 90 wt. % S content). The S/KB composite was mixed with MWCNT, super-P, and PEO/PVP in a wt. % ratio of 80: 5: 5: 10 in water. The slurry-cast sulfur cathode onto the aluminum foil consisted of 72 wt. % sulfur with a loading of 3.2 mg cm^{-2}.

Preparation of TeNW (& Te powder)-coated separator

TeNW was dispersed in water for 10 min. Pre-made 4 wt. % commercial Soteras CCS-V binder (Ashland) in an aqueous solution was added, and a CCS-B cross-linker was further added. The weight ratio between CCS-V and CCS-B was 10: 1, and the total TeNW: Binder weight % ratio was 95: 5. The final solution was kept stirring at room temperature for 30 min to obtain a homogeneous slurry. Finally, the slurry was blade casted onto one side of commercial polypropylene (PP) separator (Celgard 2500). Commercial Te powder was coated onto the separator with an analogous procedure. The Te powder-coated separator consisted of a Te: CNF: binder weight % ratio of 80: 10: 10. The coated separator was dried at 50 ºC for 5 min at atmospheric pressure.

Preparation of pre-lithiated Li-TeNW @ CNT and Li-CNT

TeNW and MWCNT were added into an ethanol : water (1:1 vol. %) solution in a weight % ratio of 10 : 90 and stir-mixed for 30 min. The obtained mixture was then intensively ultrasonicated for 30 min to form a uniform suspension. The entire solution was vacuum filtered to make the binder-free TeNW @ CNT sheet. For pre-lithiation, Li || TeNW @ CNT cells were assembled in CR-2032 type coin cells with Celgard 2500 separator and 1 M lithium bis(trifluoromethane sulfonyl)imide (LiTFSI) in 1,2-dimethoxyethane (DME) / 1,3-dioxolane (DOL) (1:1 vol. %) electrolyte. The amount of Li plated was controlled to match the N/P ratio of 1. Li-CNT was prepared in a similar method without the addition of TeNW.

Materials characterization

Morphological investigation was performed with a scanning electron microscope (FEI Quanta 650 SEM operated at 20 kV). X-ray photoelectron spectroscopy (XPS) was performed with a Kratos Analytical spectrometer with monochromatic Al Kα as a radiation source. Argon sputtering of the samples was conducted by exposing the sample surface to an Ar^+ ion beam for 10 min. A transmission electron microscope (JEOL 2010F field emission TEM) was used for obtaining high-magnification TEM images. X-ray diffraction (XRD) patterns were recorded with a Rigaku Miniflex 600 diffractometer at a scan rate of 0.5° min^{-1} with a step size of 0.02°. TGA data were collected with a thermogravimetric analyzer (Mettler-Toledo) in the temperature range of 50 – 800 ºC at a heating rate of 10 ºC min^{-1} under N_2 atmosphere.

Electrochemical cell assembly

The anode-free Ni || Li_2S full cells consisted of nickel foil as the anode substrate, separator, Li_2S-based cathodes, and 1 M LiTFSI + 0.25 M $LiNO_3$ in DME/DOL as an electrolyte. Pre-lithiated Li-CNT || S full cells were assembled with lithiated CNT sheet as the anode, separator, and S-based cathodes with the abovementioned electrolyte. All cells were assembled inside an argon-filled glovebox.

Electrochemical performance measurements

An Arbin battery cycler was used to conduct electrochemical cell cycling. For Li_2S-based anode-free cells, the cells were rested for 10 h at room temperature prior to the testing. Cells were activated at C/10 for 3 cycles between 1.8 V to 3.5 V, and the following cycles were conducted at C/5 (1.8 V – 3.0 V). 1C corresponds to a current density of 1,166 mA g^{-1} and the specific capacities were calculated based on the total Li_2S mass. For the shuttle current test, cells were initially charged to 3.5 V and then discharged to 2.35 V. After reaching 2.35 V, the voltage was maintained to record the steady-state current response resulting from the polysulfide shuttling. For S-based full cells, the cells were rested for 4 h and cycled at C/5 without activation (1C = 1,675 mA g^{-1}). Electrochemical impedance spectroscopy (EIS) measurements were performed with a Biologic VMP potentiostat in the frequency range of 1 MHz to 0.1 kHz.

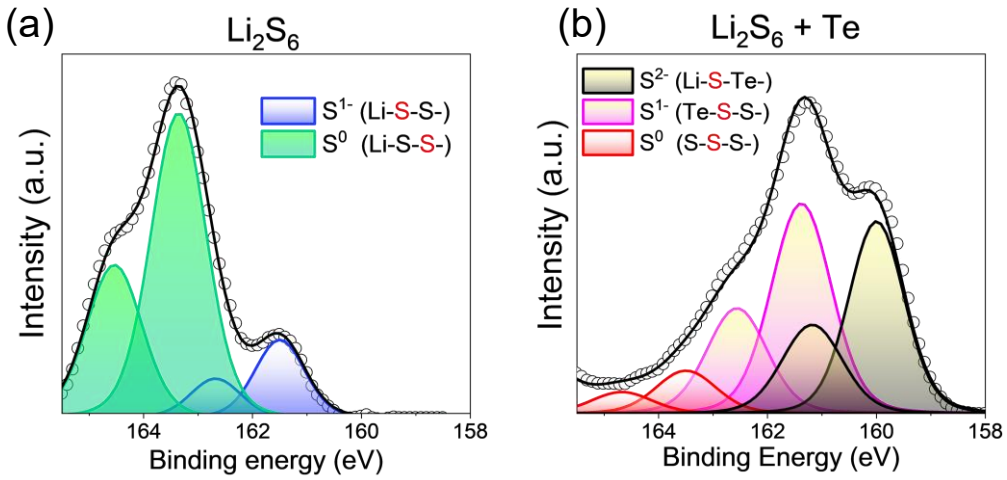

Figure S1. S 2p XPS data of Li_2S_6 and Li_2S_6 + Te at the surface. Through the reaction between Li_2S_6 and Te, S got reduced from S^0 to S^{1-} and S^{2-}.

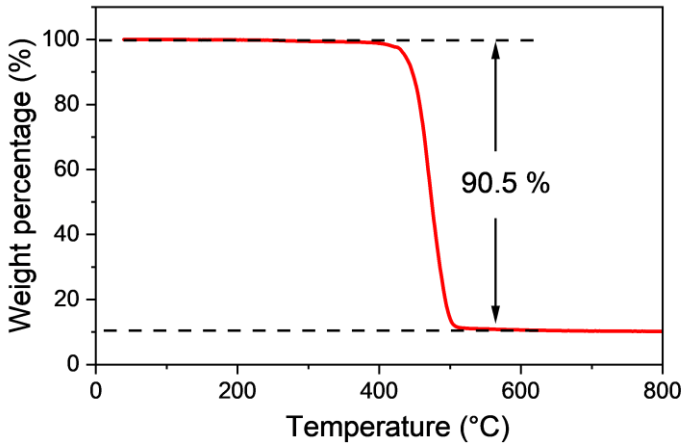

Figure S2. TGA curves in N_2 atmosphere of synthesized TeNW. TeNW yields a Te content of 90.5 and a carbon content of 9.5 wt. %.

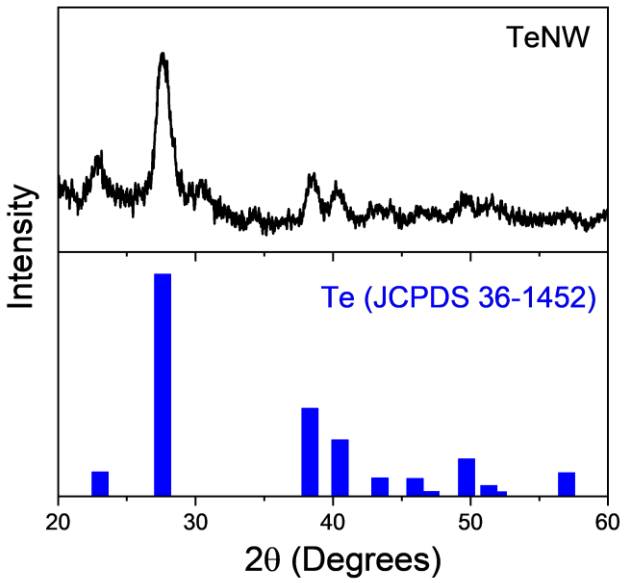

Figure S3. XRD pattern of synthesized TeNW and the reference peaks of Te.

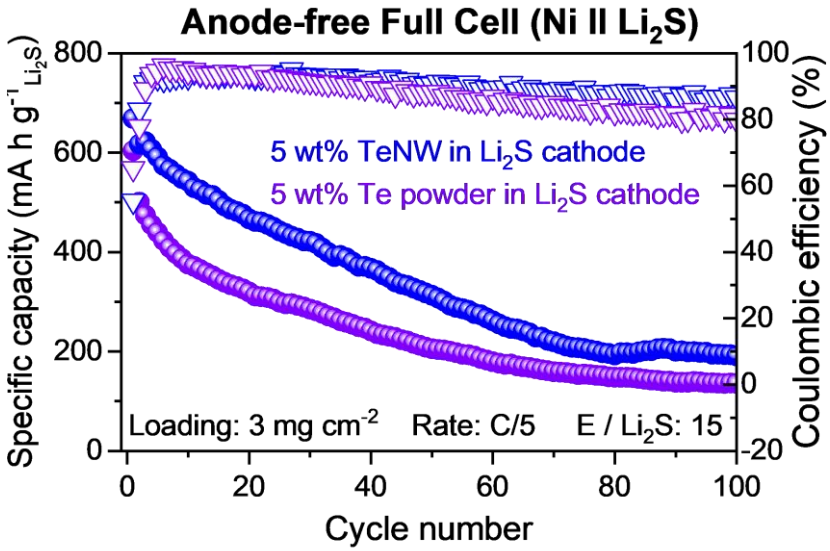

Figure S4. Long-term cycling performance of anode-free Ni || Li_2S full cells with 5 wt. % TeNW and commercial Te powder applied at the cathode.

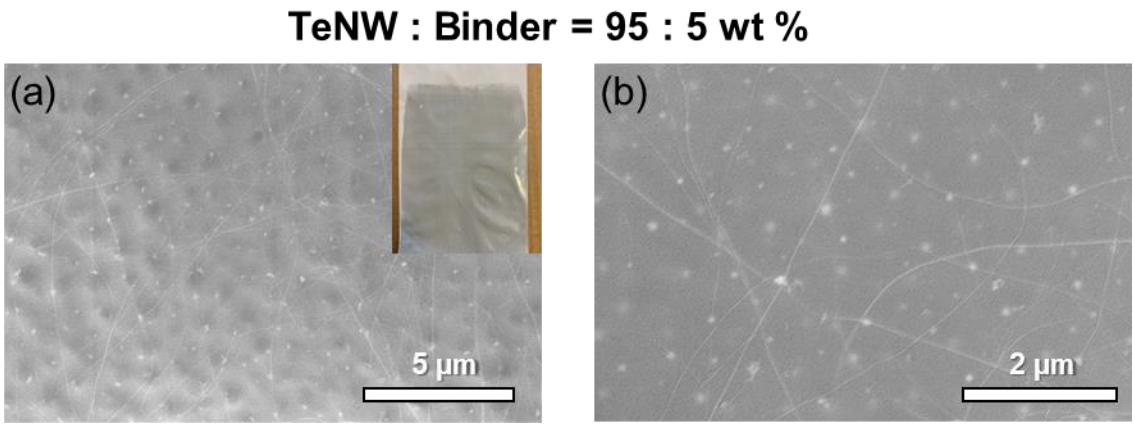

Figure S5. (a) SEM image of TeNW-coated separator. Inset: Digital image of the wide-region TeNW coating onto the separator. (b) Magnified image of TeNW on the separator.

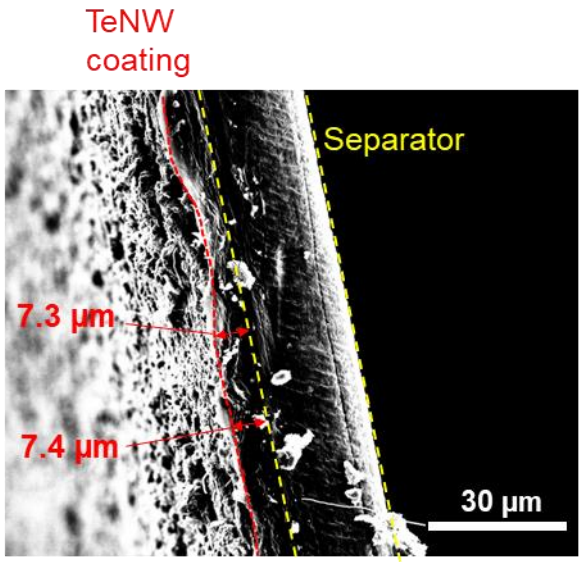

Figure S6. Cross-sectional image of TeNW-coated separator.

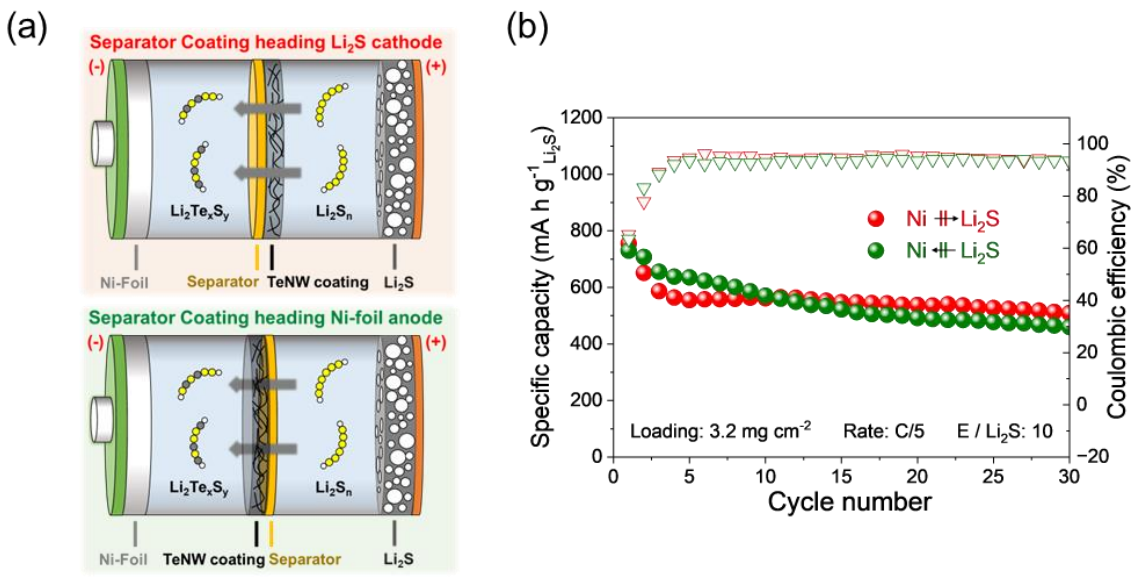

Figure S7. (a) Schematic of the two different TeNW-coated separator orientations: coated-side facing the Li_2S cathode and coated-side facing the Ni-foil anode. (b) Cell cycling performance of TeNW-coated separator facing the cathode side (red) and the anode side (green).

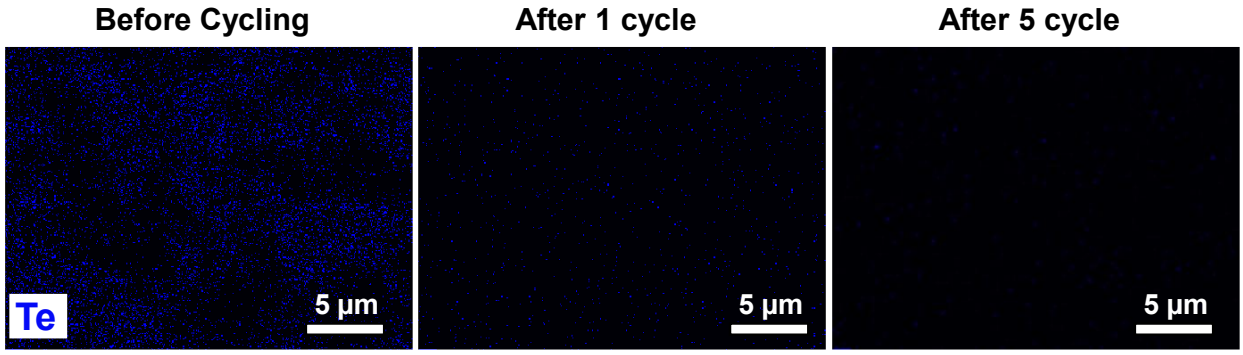

Figure S8. Elemental mapping of Te on the TeNW-coated separator before cycling, after 1 cycle, and after 5 cycles. The cycled separators were examined at the discharged state.

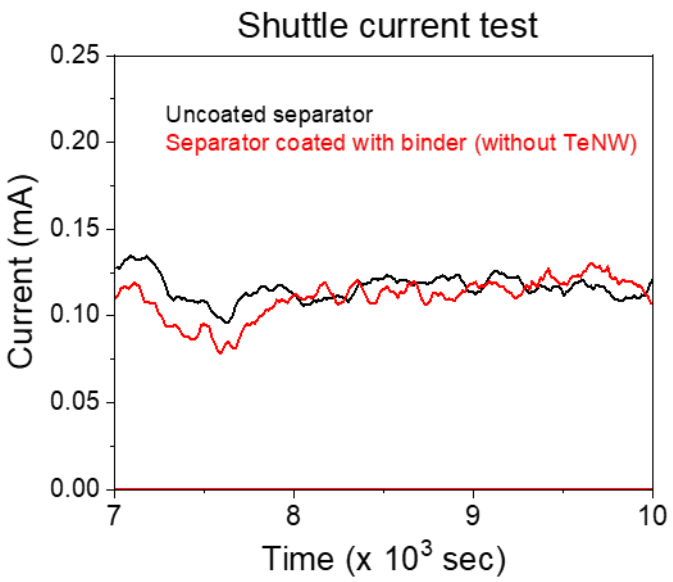

Figure S9. Shuttle current test for the uncoated separator (black) cell and for the cell in which the separator was coated only with the binder without TeNW (red). The similar shuttle current shows that the separator coating without TeNW has negligible impact on suppressing polysulfide shuttle.

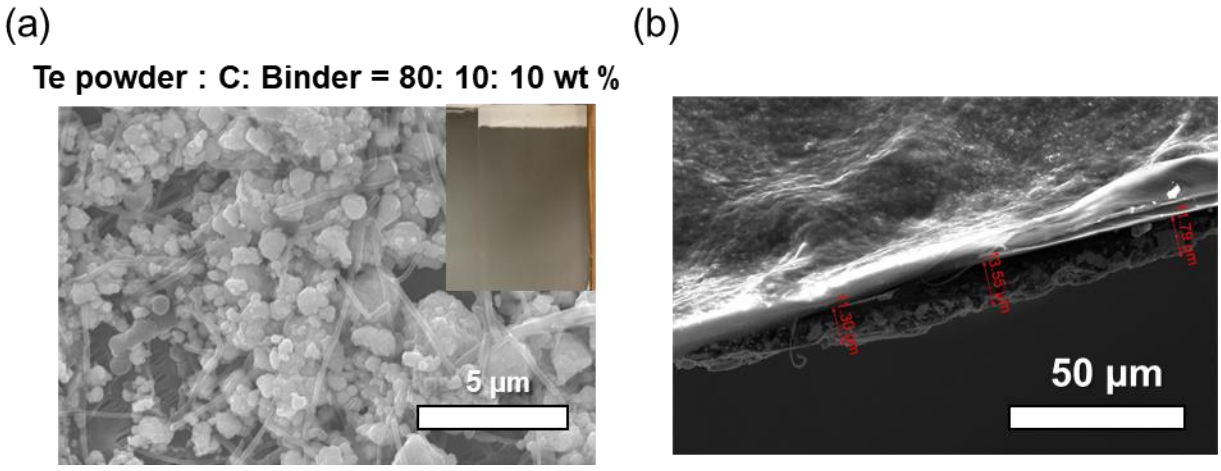

Figure S10. (a) SEM image of commercial Te powder-coated separator. Inset: Digital image of the wide-region Te powder coating onto the separator. (b) Cross-sectional image of commercial Te powder-coated separator.

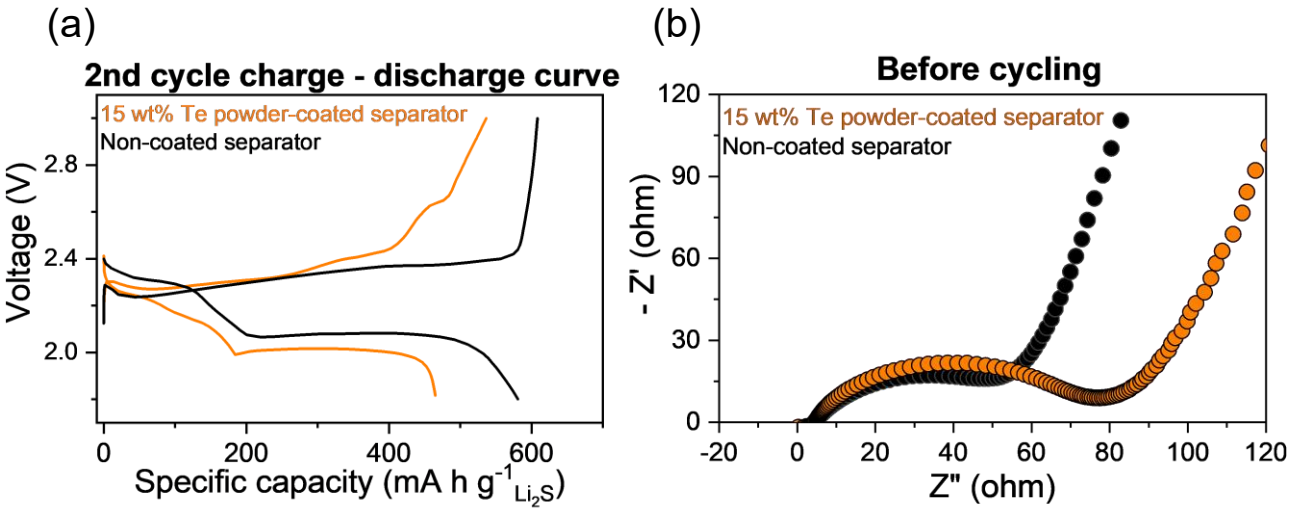

Figure S11. (a) 2nd cycle charge-discharge curves, and (b) Nyquist plots before cycling of 15 wt. % commercial Te powder-coated separator cell and uncoated separator cell.

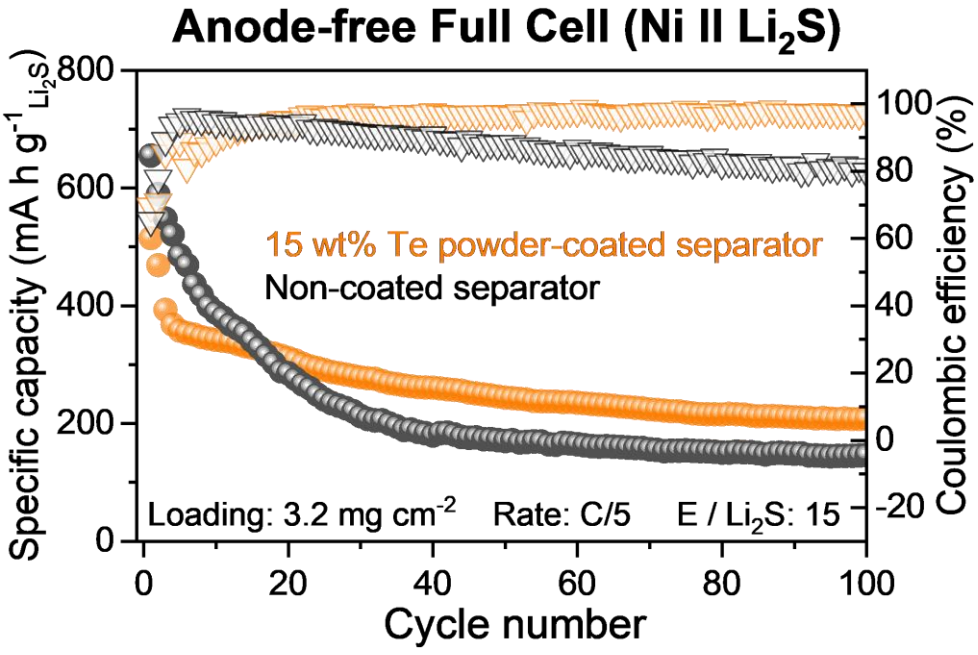

Figure S12. Long-term cycling performance of anode-free Ni || Li_2S full cells with 15 wt. % commercial Te powder-coated separator cell and uncoated separator cell.

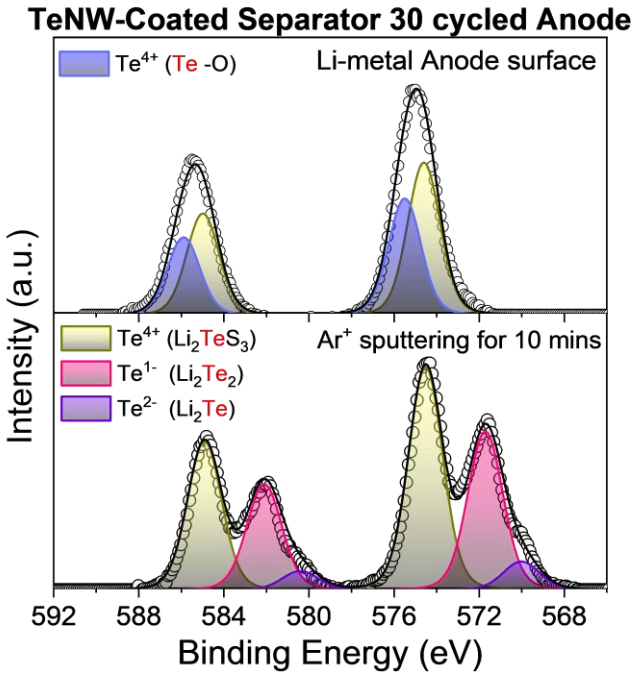

Figure S13. Te 3d XPS spectra of Li-metal surface after 30 cycles of TeNW-coated separator cell before and after Ar^+ sputtering for 10 min. The reaction mechanism and formation of polytellurosulfide species at Li-metal surface can be written as follows:

$$Te^0 + Li_2S_n \rightarrow Li_2Te_xS_y\ (Te^{4+})$$

$$Li_2Te_xS_y\ (Te^{4+}) + Li^0 \rightarrow Li_2TeS_3\ (Te^{4+})$$

$$2\ Li_2TeS_3\ (Te^{4+}) + 10\ Li^0 \rightarrow Li_2Te_2\ (Te^{1-}) + 6\ Li_2S$$

$$Li_2Te_2\ (Te^{1-}) + 2\ Li^0 \rightarrow 2\ Li_2Te\ (Te^{2-})$$

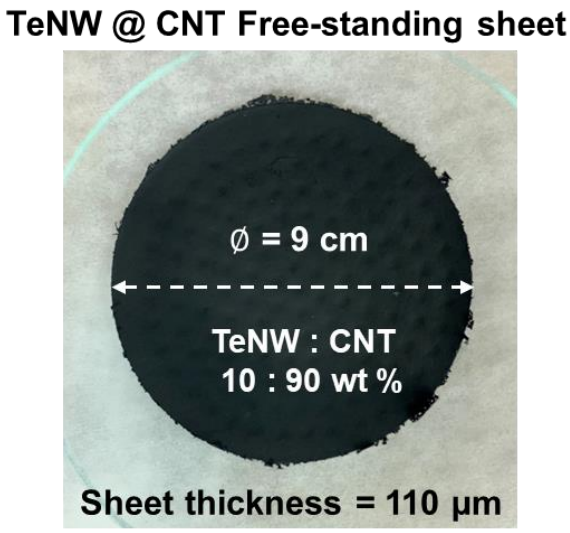

Figure S14. Digital image of vacuum-filtered TeNW @ CNT free-standing sheet.

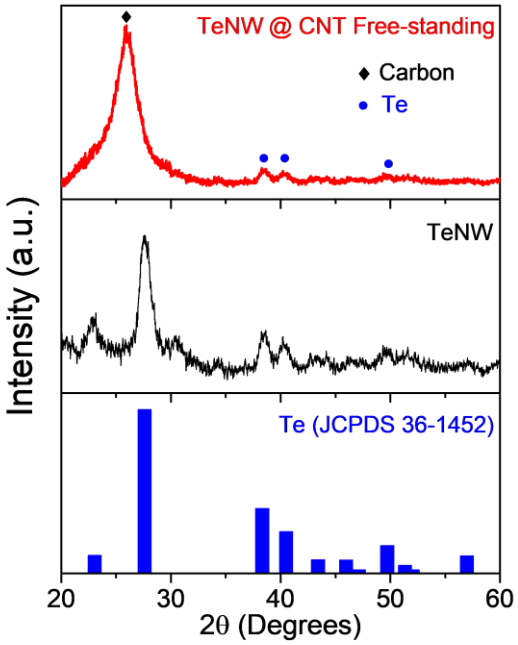

Figure S15. XRD patterns of TeNW @ CNT free-standing sheet and TeNW only, with the reference peaks of Te.

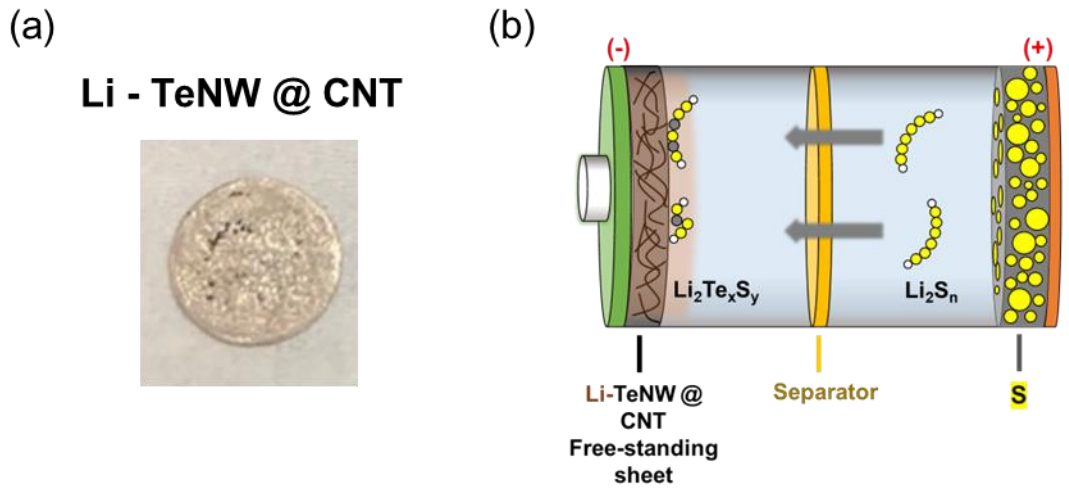

Figure S16. (a) Digital image of pre-lithiated Li-TeNW @ CNT. (b) Schematic of the Li-TeNW @ CNT || S full cell configuration. The N/P ratio was controlled to 1.

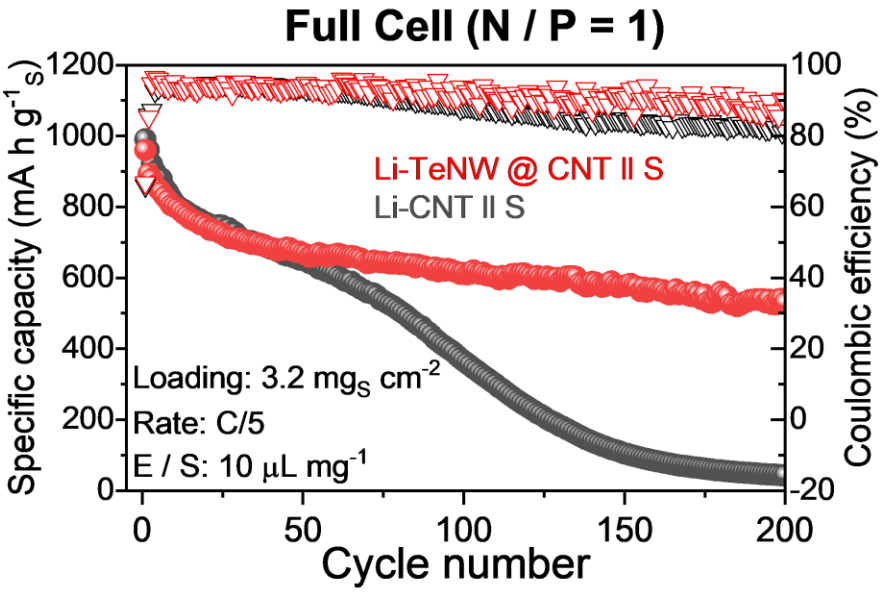

Figure S17. Long-term cycling performance of Li-TeNW @ CNT || S and Li-CNT || S full cells.

Table S1. Weight fraction contributions of each cell component in Li-S cells with practical parameters with different amounts of Te addition to the cathode compared to Li_2S

Li_2S Loading: 5 mg cm^{-2}, **Area:** 24 cm^2, **E/Li_2S:** 5 µl mg^{-1}								
Addition of Te compared to Li_2S (wt. %)	**Mass contribution (wt. %)**							
	Cathode				**Al-current collector (Cathode)**	**Separator**	**Ni-current collector (Anode)**	**Electrolyte**
	Sulfur	**Carbon**	**Binder**	**Te**				
20	11.48	2.87	1.59	2.30	3.87	2.30	9.57	66.02
10	11.62	2.90	1.61	1.16	3.92	2.32	9.68	66.79
5	11.68	2.92	1.62	0.58	3.94	2.34	9.74	67.18
0	11.75	2.94	1.63	0	3.96	2.35	9.79	67.58